

Article

Chitin-Derived Silver Nanoparticles for Enhanced Food Preservation: Synthesis, Characterization, and Antimicrobial Potential

R. Vijayaraj ¹, K. Altaff ^{1,*}, M. Jayaprakashvel ¹, R. Muthezhilan ¹, B. Saran ¹, P. Kurinjinathan ^{2,3}, Selvakumari Jeyaperumal ⁴, Venkatesan Perumal ^{5,6,*}, R. M. Saravana Kumar ⁶ and Lakshmanan Govindan ⁷

¹ Department of Marine Biotechnology, AMET University, Chennai 603112, India; vijayradha@gmail.com (R.V.); jayaprakashvel@gmail.com (M.J.); mycomuthu@gmail.com (R.M.); saranraja071@gmail.com (B.S.)

² Department of Science and Humanities (Physics), Karpagam Academy of Higher Education, Coimbatore 641021, India; nathan.pkurinji@gmail.com

³ Centre for Energy and Environment, Karpagam Academy of Higher Education, Coimbatore 641021, India

⁴ National Rural Health Mission, Integrated Disease Surveillance Programme, Directorate of Health and Family Welfare Services, Main Block of the Old Maternity Hospital, Victor Simonel Street, Puducherry 605001, India; jselvakumari87@gmail.com

⁵ Center for Injury Biomechanics, Materials, and Medicine, Department of Biomedical Engineering, New Jersey Institute of Technology, Newark, NJ 07102, USA

⁶ Department of Bioengineering, Saveetha School of Engineering, Saveetha Institute of Medical and Technical Sciences, Saveetha University, Chennai 602105, India; sarawanbio@gmail.com

⁷ Department of Anatomy, Saveetha Medical College and Hospital, Saveetha Institute of Medical and Technical Sciences, Chennai 602105, India; lakshmanang261988@gmail.com

* Correspondence: kaltaff@gmail.com (K.A.); perumal@njit.edu (V.P.)



Citation: Vijayaraj, R.; Altaff, K.; Jayaprakashvel, M.; Muthezhilan, R.; Saran, B.; Kurinjinathan, P.; Jeyaperumal, S.; Perumal, V.; Kumar, R.M.S.; Govindan, L. Chitin-Derived Silver Nanoparticles for Enhanced Food Preservation: Synthesis, Characterization, and Antimicrobial Potential. *Micro* **2023**, *3*, 912–929. <https://doi.org/10.3390/micro3040062>

Academic Editor: Nurettin Sahiner

Received: 8 October 2023

Revised: 7 November 2023

Accepted: 22 November 2023

Published: 30 November 2023



Copyright: © 2023 by the authors. Licensee MDPI, Basel, Switzerland. This article is an open access article distributed under the terms and conditions of the Creative Commons Attribution (CC BY) license (<https://creativecommons.org/licenses/by/4.0/>).

Abstract: In this research article we report the potentials of chitin-based silver nanoparticles (chitin AgNPs) derived from Indian mimic goatfish (*Mulloidichthys ayliffe*) scales as an effective food preservation agent. The study comprehensively presents the multifaceted attributes of chitin AgNPs, including their synthesis, characterization, and antimicrobial properties. Chitin yield from *M. ayliffe* scales and three-spot swimming crab (*P. sanguinolentus*) exoskeleton was determined, with the insoluble content quantified. FTIR analysis unveiled distinct absorption peaks for chitin, and scanning electron microscopy revealed the ultrastructure of chitin from both the sources. Using UV–visible spectroscopy, the biosynthesis of AgNPs was accomplished and characterized, with the color shift of the solution serving as proof of a successful synthesis. UV–vis spectra provided insights into nanoparticle size and shape. SEM micrographs exhibited spherical particle morphology, while FTIR spectra indicated amino group interactions contributing to AgNP stabilization. The antimicrobial potential of chitin AgNPs was assessed against the food pathogen, *Vibrio* spp. Chitin films displayed significant antimicrobial activity, particularly AgNP-synthesized chitin from *M. ayliffe* scales, demonstrated the highest *Vibrio* spp. inhibition activity. Furthermore, chitin AgNPs were incorporated into the common chili, *Capsicum annuum* and the tomato, *Solanum lycopersicum* to extend their shelf life at room temperature. This study reveals the efficacy of chitin AgNPs from *M. ayliffe* scales as potent agents for food preservation, offering insights into their physical, mechanical, and antimicrobial attributes. The application of chitin AgNPs to perishable food items highlights their potential in enhancing shelf life and quality, opening innovative avenues for sustainable food preservation.

Keywords: Chitin; silver nanoparticle; food preservative; *Vibrio* spp.

1. Introduction

The freshness of fruits and vegetables plays a pivotal role in shaping consumers' purchasing preferences within the market [1]. Supermarkets encounter challenges in maintaining the freshness of these products while striving to provide superior quality choices to

consumers [2]. Due to their biodegradable nature, fruits and vegetables are susceptible to microbial attacks. Swift ripening and softening makes fruits and vegetables vulnerable to decay and spoilage, severely limiting their storage, handling, and transportation capabilities. Further, preservation of these items presents challenges related to natural ripening and the degradation process, primarily driven by enzymatic reactions, which is a significant concern for the food industry [3,4].

Microbiological spoilage often leads to undesirable quality traits such as browning, off-flavor development, and textural deterioration in food products [5]. Hence, the pursuit of effective preservation methods remains a critical priority within the food industry. One promising approach is the application of biocompatible polymer coatings on fruits and vegetables [5–10]. In response to the inadequacy and high costs of traditional preservation methods, researchers have turned to natural preservatives that offer safety, efficacy, and acceptability [11]. Considering the need for extended storage and transportation times, the utilization of biologically derived preservatives that align with health and safety regulations holds great potential for preserving fruits and vegetables [4].

In order to convey active ingredients including antibrowning agents, colorants, flavors, nutrients, spices, and antibacterial substances, biopolymer coatings are specially designed. The purpose of these coatings is to extend shelf life and reduce the possibility of disease growth on food surfaces [4]. Notably, chitin emerges as an ideal candidate for preserving the freshness of fruits and vegetables due to its film-forming properties and biochemical characteristics [12]. Produce that has been coated with chitin has shown lower number of different hazardous microbes and extending the shelf life of these goods [4]. Additionally, chitin-based coatings can serve as transporters for food additives such as antimicrobials, texture enhancers, and nutraceuticals, improving the security, quality, and functionality of fruits and vegetables [13]. In recent years, amino polysaccharides derived from natural sources have found utility in biomedical applications and serve as dietary fiber sources [14,15]. Among these, chitin stands out as one of the most abundant natural polysaccharides, offering various valuable properties in foods and acting as a potential food additive [16]. Its affinity for lipids contributes to influencing lipid absorption, and it has been harnessed extensively in biomedical roles such as wound dressings as well as exhibiting antifungal and antibacterial properties [17–19]. Additionally, its capacity to absorb oxygen proves beneficial in wound and burn treatments [17]. For biomedical applications, the purity of chitin is crucial to prevent unwanted side effects, necessitating the removal of residual proteins and pigments. While chitin extraction has primarily been reported from marine crab shells and fish scales, only a limited number of studies have focused on its extraction. To address this, the present research endeavors to extract and characterize chitin from marine organisms, specifically Indian mimic goatfish (*Mulloidichthys ayliffe*) scales and three-spot swimming crab (*Portunus sanguinolentus*) shells. This study aims to establish the commercial value of chitin and assess the potential of chitin film derived from *M. ayliffe* scales and *P. sanguinolentus* shells for use as a food preservative against foodborne pathogens.

2. Materials and Methods

2.1. Collection and Identification of Experimental Specimens

The scales of *M. ayliffe* and shells of *P. sanguinolentus* were collected from the Solinganalur fish market in Chennai. Morphological characterization and identification of *M. ayliffe* and *P. sanguinolentus* were performed using resources from the FAO volumes [20]. Following collection, the samples underwent thorough washing, sun drying, and subsequent extraction of chitin through chemical methods [21].

2.2. Extraction

The powdered fish scale and crab exoskeleton samples were depolymerized chemically to obtain chitin. Deproteinization and demineralization were accomplished using

solutions of sodium hydroxide (2N) and hydrochloric acid (2N), respectively. The process of decolorization used acetone [21].

2.2.1. Deproteinization

The dried powdered scales of *M. ayliffe* and shells of *P. sanguinolentus* underwent treatment with a 2 Normality (N) sodium hydroxide (NaOH) solution at a ratio of 100 g of solid to 1000 milliliters of liquid, respectively. This mixture was stirred at 60 °C for 2 h to eliminate the proteins and other organic materials. Following the reaction, the sample was rinsed several times with distilled water and subsequently dried in a vacuum oven at 60 °C.

2.2.2. Decoloration

Further deproteinized powders were subjected to treatment with acetone at room temperature for 24 h to eliminate pigments. The cleaned powders were filtered and dried in a vacuum oven at 60 °C.

2.2.3. Demineralization

The deproteinized and decolorized material underwent treatment with a 2 N HCl solution at a ratio of 1 g solid to 15 mL liquid for 24 h at 60 °C using a magnetic stirrer. Subsequently, the powders were washed with distilled water to eliminate minerals and other soluble impurities. The resulting material obtained from prawn shells was characterized to assess the purity of the chitin.

2.3. Characterization of Chitin

Sulfated ash content and insoluble content tests were done to assess chitin production. By subtracting the weight of chitin from the powdered dry fish scale and crab exoskeleton, the chitin production was calculated. The percentage yield ((weight of chitin/weight of powder sample) × 100%) of the chitin was calculated, labeled, and stored in airtight containers until required. Chitins were dissolved in 1% of acetic acid at 25 °C and the solution was filtered. The insoluble content was calculated from the weight of chitin dissolved and the weight of insoluble particles obtained on the filter.

2.4. Characterization of the Chitin Physicochemical Properties

Instrumental methods such as scanning electron microscopy (Quanta 200 FEG ESEM), Fourier-transform infrared spectroscopy analysis, and energy-dispersive X-ray analysis were used to investigate the physicochemical properties of chitin.

2.5. Synthesis of Silver Nanoparticles using Chitin

2.5.1. Preparation of 1 mm silver nitrate (AgNO₃)

A total of 100 mL of double-distilled water was used to dissolve an exactly measured 0.017 g of AgNO₃ before being kept in an amber-colored bottle for later usage.

2.5.2. Synthesis of Silver Nanoparticles (AgNPs)

AgNPs were synthesized following the Kumaran et al. [22] method. More specifically, the chitin solution received 50 mL of freshly made AgNO₃ (1 mm). At 60 °C, the mixture was stirred for 3 h. As silver nanoparticles (AgNPs) are continuously formed throughout this period, the colour of the changed from colorless to light yellow and finally to yellowish-brown.

2.5.3. Characterization of AgNP-Mediated Chitin Nanoparticles

Utilizing a UV–visible spectrum analyzer (UV Shimadzu 1800, Shimadzu Corporation, Kyoto, Japan), a scanning electron microscope (Quanta 200 FEG ESEM, FEI Company, Hillsboro, OR, USA), and a Fourier-transform infrared spectrophotometer (Perkin Elmer FTIR model 2000 spectrophotometer, Perkin Elmer, Shelton, CT, USA), the synthesized AgNP-

medicated chitin was characterized, and particle size distribution of the chitin produced by AgNPs was determined using a particle size analyzer (Zetasizer Nano ZS, Malvern Instruments Limited, Worcestershire, UK). The morphology and crystalline structure of the powder were examined using high-resolution transmission electron microscopy (HRTEM, JEM2100F, JEOL, and Japan). For TEM observation, samples were placed onto a copper grid and dispersed in ethanol at a concentration of 1 mg/mL.

2.5.4. Preparation of Chitin Composite Film

Four distinct types of chitins (1. chitin from *M. ayliffe* scales; 2. chitin from *P. sanguinolentus* shells; 3. AgNP chitin from *M. ayliffe* scales; 4. AgNP chitin from *P. sanguinolentus* shells) were combined with starch to produce biopolymer films. Mixtures that had been homogenized were put in a sterile petri plates and immobilized with ascorbic acid. The films were left to air dry for 72 h at room temperature before being enclosed in petri dishes and kept at 4 °C for further investigation.

2.5.5. Antimicrobial Activity of Chitin Film

Bacterial cultures derived from food pathogens were received from the Marine Microbiology Laboratory, Department of Marine Biotechnology, AMET University, to evaluate the antibacterial effectiveness of the chitin films [22]. A *Vibrio* spp. broth culture was applied to nutritional agar (Himedia) plates. Pieces from the experimental and control films were placed onto the nutrient plates, where they were then incubated for 24 h at 37 °C. The presence of a definite inhibitory zone around the chitin films, confirmed the antibacterial activity.

2.6. Toxicity Assay by Hemolytic Activity

2.6.1. Preparation of RBC Suspension

Human erythrocytes were used to test the bioactive fraction's hemolytic activity. A 2.7% ethylenediaminetetraacetic (EDTA) solution was added as an anticoagulant at 5% of the blood volume after participants donated their healthy human blood. The blood was centrifuged with Phosphate Buffer Saline (PBS, pH 7.2) for 10 min at 5000 rpm. The RBC pack was resuspended in PBS after the supernatant had been removed. The supernatant was discarded following this procedure was performed three times. The study on hemolysis was conducted with 1% erythrocyte suspension [23].

2.6.2. Hemolysis Assay

The UV-vis spectrophotometer technique was used to measure hemolytic activity [24]. A 100 mM sodium phosphate buffer (100 µL to 400 µL) was used to prepare the varied concentrations of chitin sample powder before it was combined with 200 mL of blood cell solutions. A sodium phosphate buffer was eventually added in order to bring the reaction mixture volume up to 3 mL. The mixture was then heated to 37 °C for an hour in a water bath. The reaction mixture was centrifuged once more at 2500 rpm for 15 min following the incubation period. Using the sodium phosphate buffer as a blank, the optical density of the supernatant was measured at 541 nm. As a positive control, Triton X-100 was employed. The formula indicated in Equation (1) was used to compute the percentage of hemolysis.

$$\text{Inhibition activity (\%)} = \frac{\text{Abs Sample} - \text{Abs Control}}{\text{Abs Sample}} \times 100 \quad (1)$$

where Abs Control is the absorbance of Control reactions (which contain all reagents except the test sample) and Abs Sample is the absorbance of test samples. There were three duplicates of each experiment.

2.7. Applications of AgNP-Synthesized Chitin as a Food Preservative

The AgNP-synthesized chitin film from *M. ayliffe* scales exhibited the highest inhibition activity against food pathogens, indicating its potential for food preservation applications.

The chosen chitin film from *M. ayliffe* scales underwent further investigation for efficacy in preserving food, using fresh *Capsicum annuum* and *Solanum lycopersicum*. The experiments were divided into two groups: group 1, the control group, comprised fresh vegetables without the chitin film coating, and group 2, the test group, involved fresh vegetables coated with the chitin film (chitin (2 mg/mL) and starch (2 mg/mL)) blended biopolymer films were processed using glycerol as a plasticizer (100 μ L/mL). The chitin film was applied to the surface of the fresh vegetables using a dappling technique. This process involved immersing the vegetables into the chitin coating solution to ensure complete wetting of the vegetable surfaces. Afterwards, the excess coating solution was drained to remove it from the vegetable surfaces. The coated vegetables were dried to establish a firmly adhered coating on their surfaces [25]. Subsequently, the coated vegetables were kept at room temperature to assess their shelf life.

3. Results

3.1. Chitin Yield, Insoluble Content

In this study, the chitin yield obtained from 100 g of raw powder was 7.72 ± 0.04 g for *M. ayliffe* scales and 2.93 ± 0.04 g for *P. sanguinolentus* exoskeleton. The percentage of insoluble content in chitin was found to be $20.66 \pm 0.94\%$ for *M. ayliffe* and $90.33 \pm 0.47\%$ for *P. sanguinolentus* (Table 1).

Table 1. Yield, insoluble content in chitin and protein content of chitin.

Name of the Sample	Yield (g)	Insolubility Content (%)
<i>M. ayliffe</i>	7.72 ± 0.04	20.66 ± 0.94
<i>P. sanguinolentus</i>	2.93 ± 0.04	90.33 ± 0.47

3.2. UV–vis Spectroscopy Analysis of Chitin

The UV spectrum of chitin shows an absorption band between 300 nm and 400 nm, with a maximum absorption of 350 nm for both extracted from *M. ayliffe* scales and from *P. sanguinolentus* exoskeleton (Figure 1).

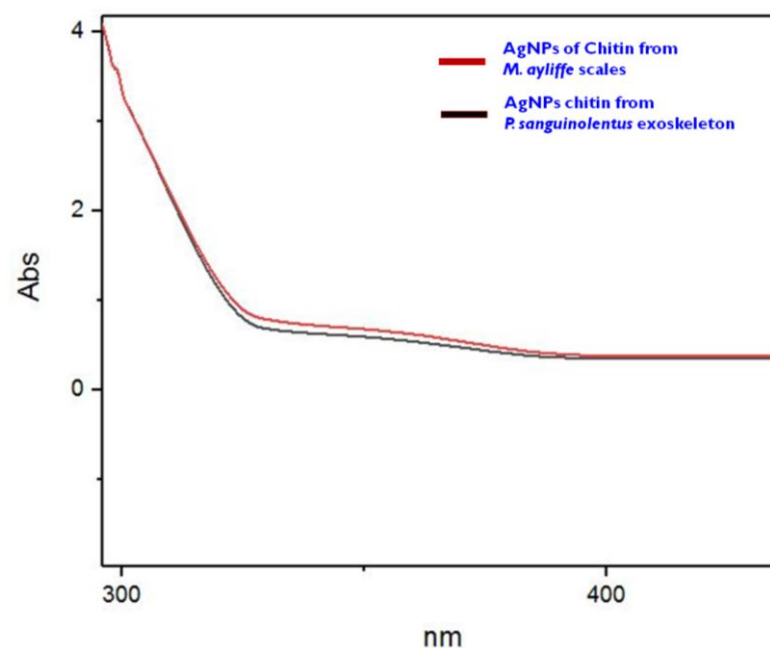


Figure 1. UV–vis spectrum of chitin.

3.3. FTIR Analysis of Chitin

The FTIR spectrum analysis of chitin from *M. ayliffe* shells exhibited characteristic absorbance peaks at 3490 cm^{-1} , 1700 cm^{-1} , 1400 cm^{-1} , and 1100 cm^{-1} . These peaks correspond to O–H stretching, C=O stretching, N–O asymmetric stretching, and C–N stretching, respectively. Similarly, the FTIR spectrum of *P. sanguinolentus* exoskeleton displayed absorbance peaks at 2900 cm^{-1} , 1700 cm^{-1} , 1400 cm^{-1} , and 1100 cm^{-1} , associated with H–C=O:C–H stretch, C=O stretch, N–O asymmetric stretch, and C–N stretch, respectively (Figure 2 & Table 2).

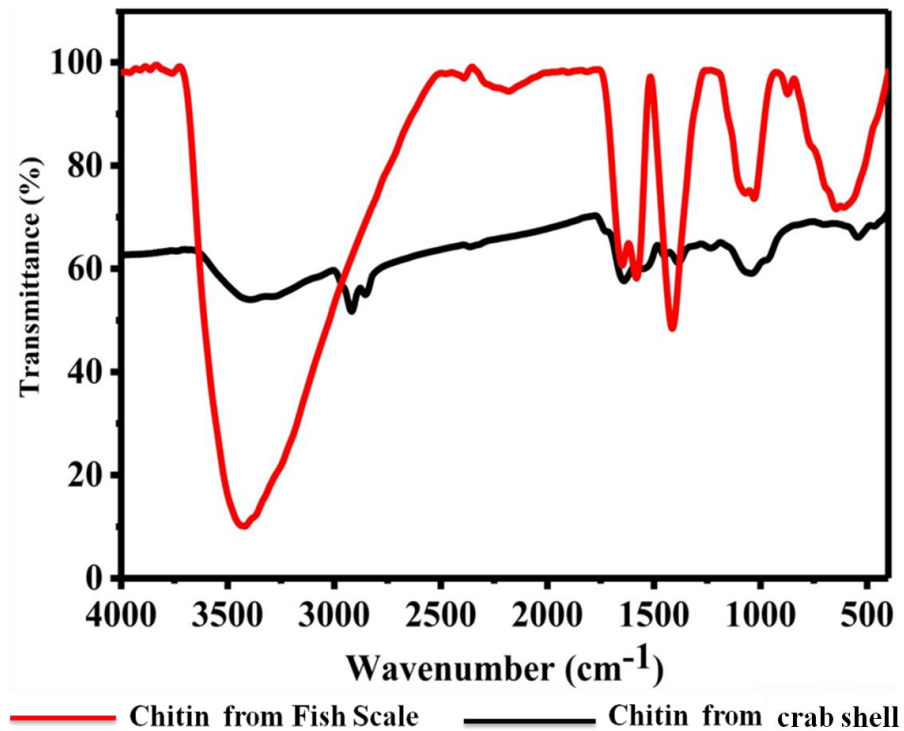


Figure 2. FTIR spectrum of chitin.

Table 2. FTIR spectrum of chitin.

Frequency, cm^{-1}	Bond	Functional Group
Chitin from <i>M. ayliffe</i> scales		
3490	O–H stretch	Alcohols
1700	C=O stretch	Carbonyls
1400	N–O asymmetric stretch	Nitro compounds
1100	C–N stretch	Aliphatic amines
Chitin from <i>P. sanguinolentus</i> exoskeleton		
2900	H–C=O: C–H stretch	Aldehydes
1700	C=O stretch	Carbonyls
1400	N–O asymmetric stretch	Nitro compounds
1100	C–N stretch	Aliphatic amines

3.4. SEM Analysis of Chitin

The ultrastructure of chitin extracted from *M. ayliffe* scales and *P. sanguinolentus* exoskeleton is depicted in Figures 3 and 4, respectively. Both the samples exhibited long and thin crystal structures with smooth surface morphologies under scanning electron microscopic examination.

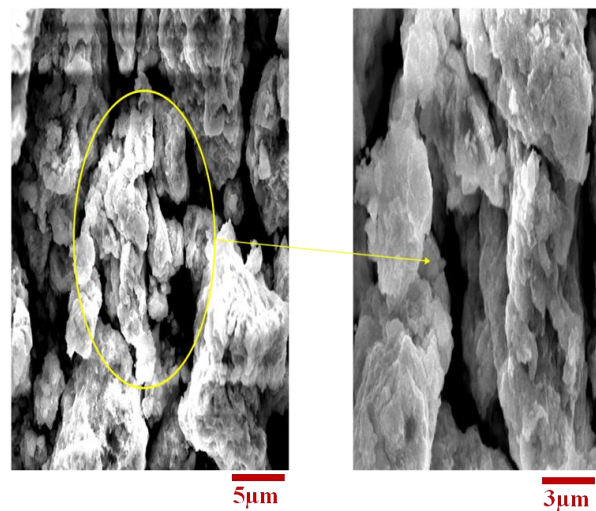


Figure 3. SEM of chitin from *M. ayliffe* scales.

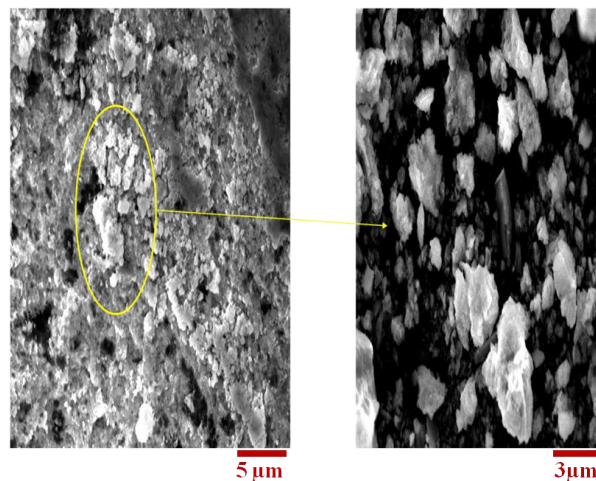


Figure 4. SEM of chitin from *P. sanguinolentus* exoskeleton.

3.5. Synthesis and Characterization of Silver Nanoparticles

UV–visible spectroscopy was used to characterize the biosynthesized AgNPs. AgNPs were successfully synthesized when the color of the solution changed from colorless to light yellow to yellowish-brown as the synthesis progressed. The AgNO₃ surface plasmon resonance's (SPR) excitation is what was responsible for the color change that happened gradually. The solution's spectral absorption pattern between 300 and 700 nm was observed (Figure 5). To evaluate the nanoparticles' size and form, UV–vis spectroscopy was used. In the analysis of the UV–vis spectrum, a noteworthy absorbance peak with a wavelength falling within the range of 370 to 424 nm was observed. This distinct peak was observed in the spectrum of AgNPs that were synthesized using chemically extracted chitin obtained from both *M. ayliffe* scales and *P. sanguinolentus* exoskeleton. The UV–vis spectrum, as depicted in Figure 5, clearly exhibited this characteristic absorbance feature, indicating the presence of AgNPs with specific optical properties. To further investigate the morphology of the synthesized AgNPs, scanning electron microscope (SEM) imaging was employed. The acquired SEM micrographs, shown in both Figures 6 and 7, revealed the predominant presence of particles displaying a spherical shape. This observation is in line with the anticipated morphology of nanoparticles. The SEM images provided a visual insight into the physical structure of the AgNPs and corroborated the findings from the UV–vis spectrum, enhancing our understanding of the synthesized nanoparticles' characteristics. The surface topography and ultrastructure of the chitin films made by chemical techniques

are shown in the SEM micrographs. Under scanning electron microscopy, the chitin of both samples displayed a long, thin crystal structure with a smooth surface appearance.

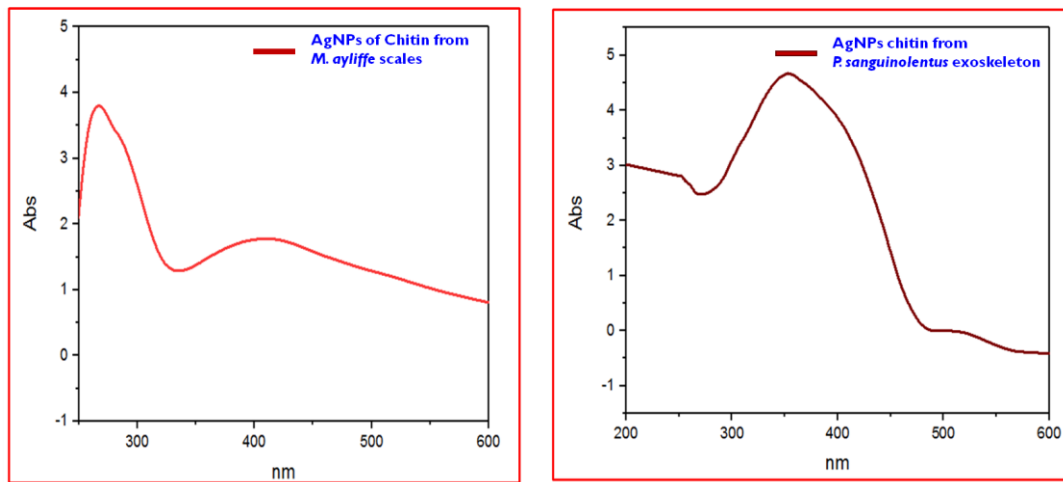


Figure 5. UV-vis spectrum analysis of chitin AgNPs.

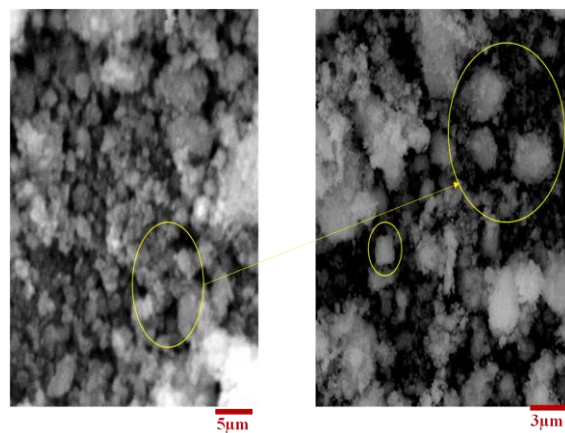


Figure 6. SEM of chitin AgNPs from *M. ayliffe* scales.

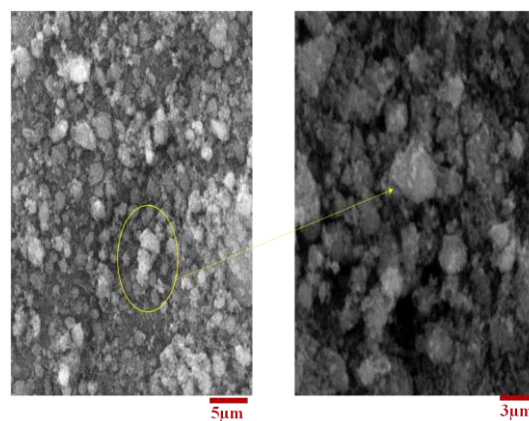


Figure 7. SEM of chitin AgNPs of *P. sanguinolentus* exoskeleton.

Furthermore, the Fourier-transform infrared (FTIR) spectrum demonstrated absorption peaks within the range of 3200, 2700, 1500, 1000, and 900 for AgNPs synthesized from *M. ayliffe* scales, indicative of H-bonded, H-C=O: C-H stretching, N-O asymmetric stretching, =C-H bending, and C-H bonding, respectively. For AgNPs synthesized from *P. sanguinolentus* exoskeleton, significant peaks were detected at 3400, 1700, 1600, and 1000,

signifying H-bonded interactions, C=O stretching, N–O asymmetric stretching, and =C–H bending (Figure 8 & Table 3).

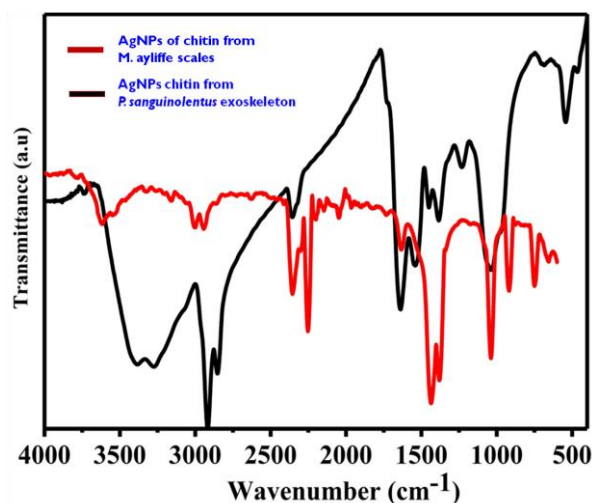


Figure 8. FTIR analysis of chitin AgNPs.

Table 3. FTIR analysis of chitin AgNPs.

Frequency, cm^{-1}	Bond	Functional Group
Chitin from <i>M. ayliffe</i> scales		
3200	H-bonded	Alcohols
2700	H–C=O: C–H stretch	Aldehydes
1500	N–O asymmetric stretch	Nitro compounds
1000	=C–H bend	Aalkenes
900	C–H	Aromatics
Chitin from <i>P. sanguinolentus</i> exoskeleton		
3400	H-bonded	Alcohol
1700	C=O stretch	Aldehyde and Ketone
1600	N–O asymmetric stretch	Nitro compounds
1000	=C–H bend	Aalkenes

UV–visible spectroscopy was used to characterize the biosynthesis of AgNPs. Visual observation revealed that the color of the solution changed from colorless to light yellow and then to yellowish-brown, which supported the synthesis of AgNPs. The excitation of AgNO_3 's surface plasmon resonance (SPR) is what caused the intensity of the yellowish-brown color to increase. Without chitin, the AgNO_3 solution used as a control exhibited no color change. Kinetic measurements were made of the solution's light absorption pattern between 300 and 700 nm. Examining NPs with regulated size and form could be performed using UV–vis spectroscopy. The distinctive absorbance peak was seen at 424 nm in the UV–vis spectra of AgNPs made from chemically removed chitin from the exoskeletons of *P. sanguinolentus* and *M. ayliffe* scales. The AgNPs synthesized from the chitin of *M. ayliffes* scales exhibited absorption peaks at approximately between the range of 3200 cm^{-1} , 2700 cm^{-1} , 1500 cm^{-1} , 1000 cm^{-1} , and 900 cm^{-1} , which is indicative of the H-bonded, H–C=O: C–H stretch, N–O asymmetric stretch, =C–H bend, and C–H band, respectively. The SEM micrographs primarily showed that H-bonded, C=O stretch, N–O asymmetric stretch, and =C–H bend were all indicated by prominent peaks at 3400, 1700, 1600, and 1000 in the AgNPs synthesized from *P. sanguinolentus*. The findings clearly show that the main amino groups were involved in the interaction with metal surfaces and that these groups served as capping sites for the stabilization of AgNPs. The FTIR spectra of chitin derived from various sources were examined in the present study. As a result of O–H stretching, C=O stretching, N–O asymmetric stretching, and C–N stretching, respectively, chitin from *M. ayliffe* scales showed absorbance peaks at 3490 cm^{-1} , 1700 cm^{-1} , 1400 cm^{-1} ,

and 1100 cm^{-1} . Similar to this, the chitin from the exoskeleton of *P. sanguinolentus* showed peaks at 2900 , 1700 , 1400 , and 1100 cm^{-1} , which corresponded to H-C=O:C-H stretching, C=O stretching, N-O asymmetric stretching, and C-N stretching. Peaks in chitin from *Brachytrupes portentosus* were seen at 3433 cm^{-1} , $3257\text{--}3103\text{ cm}^{-1}$, 1653 cm^{-1} , 1622 cm^{-1} , 1554 cm^{-1} , and 1311 cm^{-1} , which were in agreement with the results of the present study.

With reference to the particle analysis of the AgNP-synthesized chitin, the Poly Dispersive Index value has been found to be 1 for AgNP-synthesized chitin from *M. ayliffe* scales; the sample has uniform size distribution in the range of $60\text{--}100\text{ nm}$ and PDI is greater than 0.7 for AgNP-synthesized chitin from *P. sanguinolentus*, which shows the samples having broad size distribution of $90\text{--}130\text{ nm}$ (Figure 9). The findings of the investigation supported the size distribution of synthesized AgNPs in the nanosize range with average particle diameter. Furthermore, the sample-synthesized chitin from *M. ayliffe* scales showed narrow and low size distribution, and it was subjected to HR-TEM analysis for more insights.

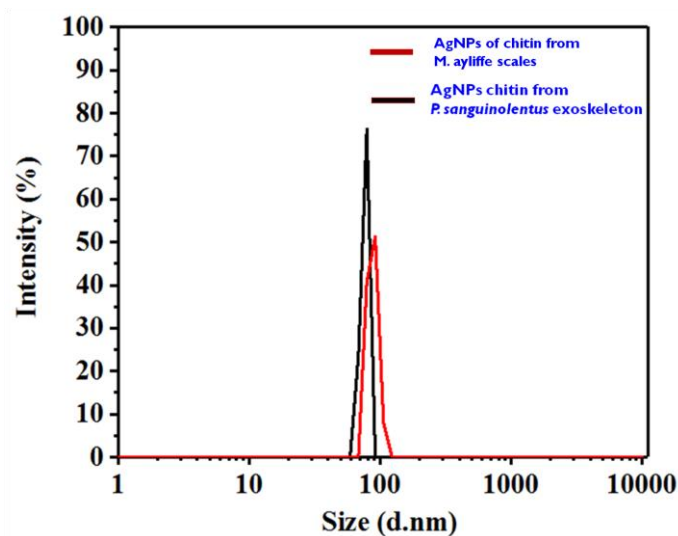


Figure 9. DLS analysis of AgNP-synthesized chitin.

TEM micrographs of the AgNP-synthesized chitin from *M. ayliffe* scales are shown in Figure 10a,b, and Figure 10c,d show the HR TEM and SAED patterns of AgNP-synthesized chitin from *M. ayliffe* scales. However, the micrographs showed agglomerated rod like nanoparticles for both samples. Figure 10a shows a variation of size ranging from $15\text{--}70\text{ nm}$ in length and $5\text{--}10\text{ nm}$ in breadth. Figure 10c shows that the particle has lattice fringes with a certain orientation on the particle surface that indicates the atomic distance between two adjacent atoms in the crystal structures of silver. The lattice interface is measured to be $\sim 2.9\text{ \AA}$, which corresponds to (111) fcc single crystal plane of an Ag crystal. The interference lines shown on every single particle indicate that the atoms were subjected to distortion during the reaction of the SAED pattern from Ag powder. A transmission electron microscope (TEM) can be used for SAED, a crystallographic experimental method. The image clearly shows a bright circle of dots, each of which corresponds to a sample's crystal structure's satisfied diffraction requirement. The same crystal will remain illuminated when the sample is tilted, but distinct diffraction conditions will be activated, causing different diffraction spots to form or vanish. The pattern's spotted circles correspond to the Ag structure's pure phase. The pattern is indexed to the fcc silver values (111), (200), (220), (311), and (222), respectively. Additionally, these patterns demonstrated the polycrystalline nature of Ag powder. Further, results of the Zeta potential of AgNP-synthesized chitin is presented in Figure 11. Subsequently, the synthesized silver nanoparticles were integrated into the fabrication of a chitin composite film and subjected to further characterization. The antimicrobial potential of the composite film against the food borne pathogen *Vibrio* spp. was also investigated.

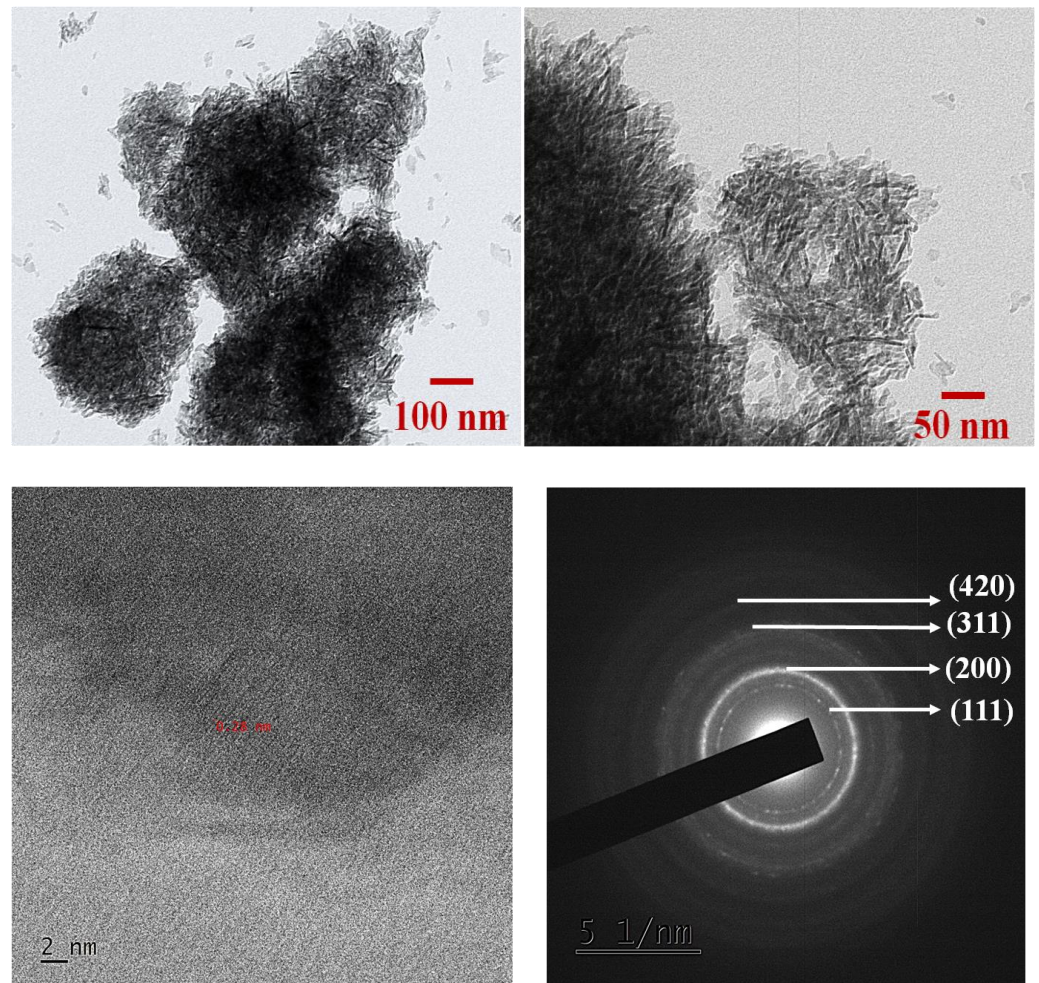


Figure 10. TEM analysis of AgNP-synthesized chitin from *M. ayliffe* scales.

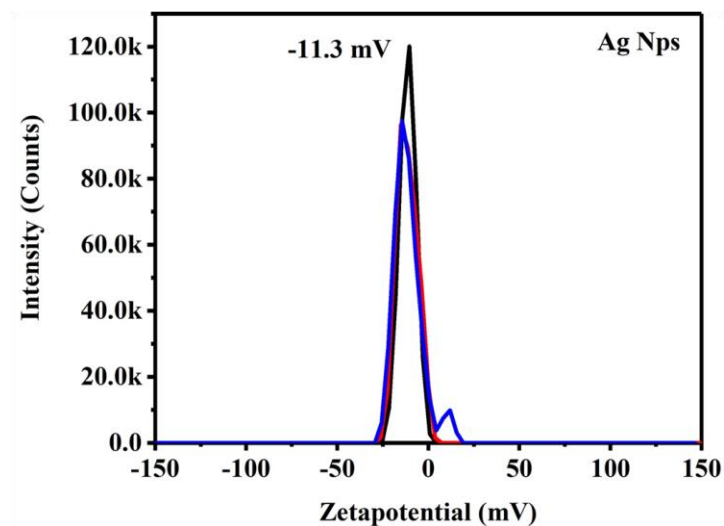


Figure 11. Zeta potential analysis of AgNP-synthesized chitin.

3.6. Toxicological Assessment of AgNP-Synthesized Chitin from *M. ayliffe* Scales

As for the hemolytic effects of silver nanoparticles (AgNPs) synthesized from chitin from *M. ayliffe* scales on human erythrocytes, the results indicate a concentration-dependent increase in the percentage of hemolysis, suggesting that as the concentration of AgNPs rose, so did the damage to the red blood cells (RBCs). Surprisingly, when comparing

concentrations of 200, 400, and 600 $\mu\text{g}/\text{mL}$ of AgNPs, no substantial variation in the degree of hemolysis was observed. However, the positive control used in the study exhibited the highest level of RBC hemolysis. The hemolysis caused by the AgNPs was found to be 4.54% of what was observed in the hemolysis induced by the positive control, as represented in Figure 12. This outcome suggests that while the hemolysis increased with rising AgNP concentrations, the levels remained notably lower (4.54%) than the positive control, indicating a relatively low impact on RBCs. Overall, these findings indicate that while AgNPs synthesized from chitin from *M. ayliffe* scales caused concentration-dependent hemolysis, the levels were notably low compared to the control substance or condition.

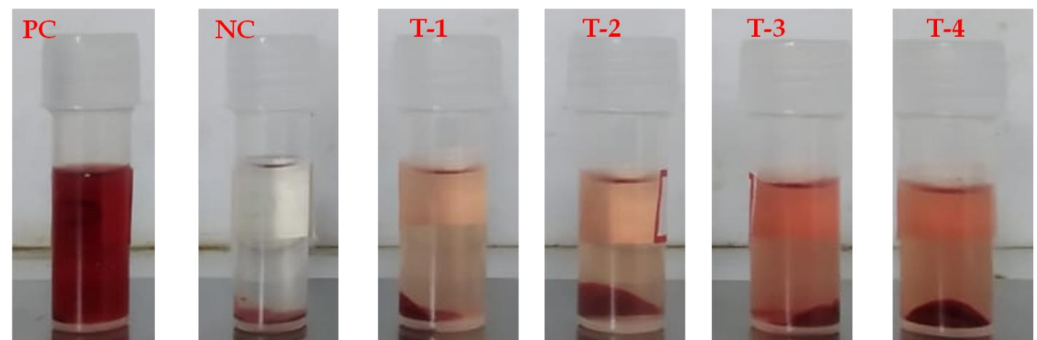


Figure 12. Hemolysis assay of AgNP-synthesized chitin from *M. ayliffe* scales. (Positive Control—Triton \times 100; Negative Control—Phosphate Buffer Saline); (Tested Sample—T-1: 100 $\mu\text{g}/\text{mL}$ AgNPs chitin from *M. ayliffe* scales; T-2: 200 $\mu\text{g}/\text{mL}$ AgNPs chitin from *M. ayliffe* scales; T-3: 300 $\mu\text{g}/\text{mL}$ AgNPs chitin from *M. ayliffe* scales; T-4: 400 $\mu\text{g}/\text{mL}$ AgNPs chitin from *M. ayliffe* scales).

3.7. Antimicrobial Activity of Chitin Film against Food Pathogen *Vibrio* spp.

The foodborne pathogen *Vibrio* spp. was significantly inhibited by the antimicrobial action of the chitin films. *M. ayliffe* scales, *P. sanguinolentus* exoskeleton, AgNP-synthesized chitin from *M. ayliffe* scales, and AgNP-synthesized chitin from *P. sanguinolentus* were the four different chitin films (Figure 13). Tested for their antimicrobial potential, AgNP-synthesized chitin from *M. ayliffe* scales displayed the highest level of inhibitory activity, measuring 20 mm (Table 4). This was in comparison to the other films in their effectiveness against the *Vibrio* spp. foodborne pathogen. This segment succinctly reiterates the outcomes of the antimicrobial testing of the chitin films against the *Vibrio* spp. food pathogen. It effectively conveys the heightened inhibitory action of AgNP-synthesized chitin from *M. ayliffe* scales when compared to the other chitin film variants, underscoring its potential as an effective agent against the targeted foodborne pathogen.

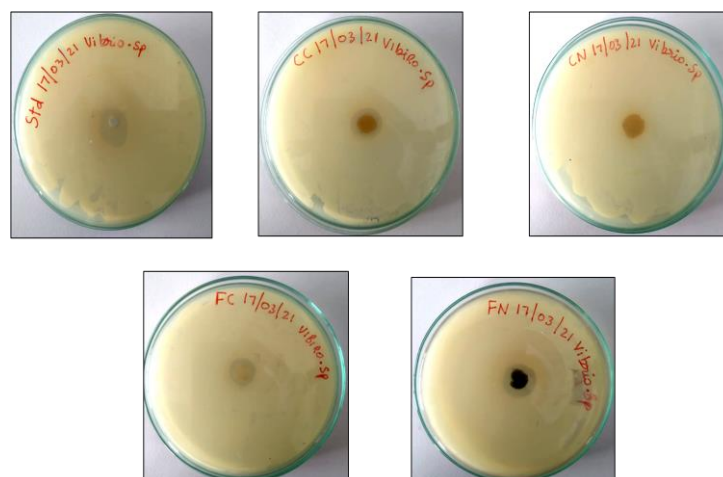


Figure 13. Antimicrobial activity of chitin films against *Vibrio* spp.

Table 4. Antimicrobial activity of chitin films against *Vibrio* spp.

Standard (Tetracycline)	Zone of Inhibition (mm)			
	Chitin from <i>M. ayliffe</i> Scales	Chitin from <i>P. sanguinolentus</i> Exoskeleton	AgNPs from <i>M. ayliffe</i> Scales Chitin	AgNPs from <i>P. sanguinolentus</i> Exoskeleton Chitin
22 ± 0.74	15 ± 0.48	15 ± 0.92	20 ± 1.67	10 ± 0.45

3.8. Exploring Chitin AgNPs from M. ayliffe Scales for Food Preservation

In the scope of the current research, we delved into the potential applications of chitin-based silver nanoparticles (Chitin AgNPs) derived from *M. ayliffe* scales as effective agents for food preservation. The study delves into the multifaceted attributes of Chitin AgNPs from *M. ayliffe* scales, including their physical, mechanical, and antimicrobial properties. The findings suggest that these nanoparticles may hold promise for enhanced food preservation. The approach involved coating chitin AgNPs from *M. ayliffe* scales onto the outer layers of *Capsicum annuum* and *Solanum lycopersicum*, two commonly consumed vegetables. This coating process was meticulously conducted under sterile conditions at ambient room temperature to ensure the integrity and purity of the nanoparticles. The results reveal that when compared to non-coated chitin nanoparticles, the chitin nanoparticle-coated *Capsicum annuum* and *Solanum lycopersicum* demonstrated a notable extension in shelf life, ranging from 0 to 5 days, when stored at room temperature (Figure 14). This finding underscores the potential of chitin AgNPs from *M. ayliffe* scales as effective food preservatives, showcasing their ability to mitigate natural processes of decay and spoilage. These observations shed light on the augmented preservation capabilities offered by chitin AgNPs from *M. ayliffe* scales, particularly when applied to perishable food items. The implications of these findings extend to the field of food technology, offering innovative avenues for sustainably enhancing the shelf life and quality of consumables.

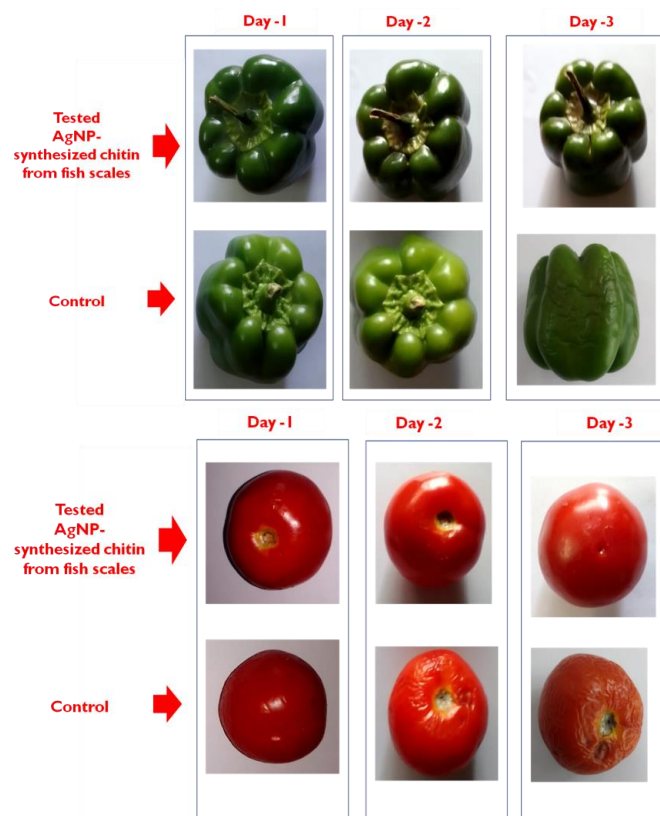


Figure 14. Shelf-life period of chitin nanoparticle-coated *C. annuum* and *S. lycopersicum*.

In the present study, chitin AgNPs from *M. ayliffe* scales showed potential physical, mechanical, and antimicrobial properties. Of the many nanoparticles tested, chitin AgNPs of *M. ayliffe* scales showed better food preservative applications. The chitin silver nanoparticles of *M. ayliffe* scales were coated as an outer layer on *C. annuum* and *S. lycopersicum* under sterile conditions at room temperature. The result indicates that when compared to chitin nanoparticle non-coated *C. annuum* and *S. lycopersicum*, chitin nanoparticle-coated *C. annuum* and *S. lycopersicum* showed a good shelf life (0 to 5 days) at room temperature.

4. Discussion

As the most prevalent renewable polymer in the oceans and a vital source of carbon and nitrogen for marine species, chitin is extraordinary. The breakdown of chitin is essential for the nutrient cycle in marine habitats. Chitinolytic bacteria significantly impact this breakdown process. In a recent study, it was discovered that 2.930.04 g of *P. sanguinolentus* exoskeleton and 7.720.04 g of *M. ayliffe* scales yielded the most chitin per 100 g of raw powder. Chitin's complex structure, combined with its low solubility, makes it difficult to use, especially in pharmacology. To combat this, significant attempts have been made to improve chitin's solubility by changes to its chemical make-up. A greater range of applications for chitin could result from increased solubility. In addition, chitin synthesis has drawn more attention lately [26]. Due to chitin's positive and helpful biological features, there has been an increase in interest in recent years in extracting it from various sources for medical purposes [22,27]. In this respect, it is important to note that chitin isolated from *M. ayliffe* has an approximate insoluble content percentage of 20.660.94%, whereas *P. sanguinolentus* has a significantly higher insoluble content percentage of 90.330.47%. Similarly, Vijayaraj et al. [22] emphasized the yield and insoluble content of the chitin from *C. gracilirostris*. The FTIR spectra of chitin derived from various sources were examined in this work. As a result of O–H stretching, C=O stretching, N–O asymmetric stretching, and C–N stretching, respectively, chitin from *M. ayliffe* scales showed absorbance peaks at 3490 cm^{-1} , 1700 cm^{-1} , 1400 cm^{-1} , and 1100 cm^{-1} . Similar to this, the chitin from the exoskeleton of *P. sanguinolentus* showed peaks at 2900 cm^{-1} , 1700 cm^{-1} , 1400 cm^{-1} , and 1100 cm^{-1} , which corresponded to H–C=O:C–H stretching, C=O stretching, N–O asymmetric stretching, and C–N stretching. Peaks in chitin from *Brachytrupes portentosus* were seen at 3433 cm^{-1} , 3257–3103 cm^{-1} , 1653 cm^{-1} , 1622 cm^{-1} , 1554 cm^{-1} , and 1311 cm^{-1} , which were in agreement with the results of the present study. Furthermore, similar absorbance peaks were shared by chitin from different sources like *Bombyx mori* [28], *Cicada sloughs* [29], Orthoptera sp. [21], and *Parapenaeus longirostris* prawn exoskeleton [30]. Comparatively, Povea et al. [31] found absorption peaks at wavelengths of 3450 cm^{-1} , 1870–2880 cm^{-1} , 1655 cm^{-1} , 1580 cm^{-1} , and 1320 cm^{-1} , which were attributed to O–H stretching, CH–stretching, Amide I, –NH₂ bending, and Amide III, respectively. In addition, absorption bands were found at 1160 cm^{-1} (C–O–C bridge), 1082 and 1032 cm^{-1} (C–O stretching), 896 and 894 cm^{-1} (saccharide rings), and 600–500 cm^{-1} (alkyl halides). Similar bands relating to –OH, –NH₂, and –CO groups were visible in the chitin of the shrimp exoskeleton at 670, 700, and 1000 cm^{-1} , which is a sign of N-acetylation. Overall, the literature suggests strong interactions between sugar chains and solvent in chitin's long-chain polymer structure, highlighted by widened bands corresponding to –NH₂, –OH (3390–3418 cm^{-1}), C=O (1716–1724 cm^{-1}), amide I (1626–1633 cm^{-1}), amide II (1520–1531 cm^{-1}), C3–OH (double peaks, 1178–1189 cm^{-1} and 1148–1153 cm^{-1}), C6–OH (1073–1074 cm^{-1}), 897 cm^{-1} (C–O–C bridge and glycosidic linkage), and 700–610 cm^{-1} (–C≡C–H:C–H), 690–515 cm^{-1} (C–Br stretch). According to the FTIR results of the current study [32–36], this closely matches the chemical composition and bonding types of commercially available chitin.

Numerous scientific domains have made extensive use of noble metal nanoparticles, particularly silver nanoparticles [32]. Chemistry, biology, healthcare, electronics, and other related fields should all pay close attention to their special properties because they can be used to create biosensor materials, composite fibers, cosmetic products, antimicrobial applications, conducting materials, and electronic components [28]. A comprehensive

application and area of use perspective makes understanding the silver nanoparticle production processes crucial [37]. The control of their physical properties, such as obtaining uniform particle size distribution, identical shape, morphology, nanoparticle coating or stabilizing agent, chemical composition or type, and crystal structure, is the main challenge in the synthesis of silver nanoparticles [38]. As a result, in the current study, chitin was used to create silver nanoparticles for uses in food preservation.

UV–visible spectroscopy was used to characterize the biosynthesis of AgNPs. Visual observation revealed that the color of the solution changed from colorless to light yellow and then to yellowish-brown, which supported the synthesis of AgNPs. The excitation of AgNO₃'s surface plasmon resonance (SPR) is what caused the intensity of the yellowish-brown color to increase. Without chitin, the AgNO₃ solution used as a control exhibited no color change. Kinetic measurements were made of the solution's light absorption pattern between 300 and 700 nm. Examining NPs with regulated size and form could be performed using UV–vis spectroscopy. The distinctive absorbance peak was seen at 424 nm in the UV–vis spectra of AgNPs made from chemically-removed chitin from the exoskeletons of *P. sanguinolentus* and *M. ayliffe* scales. The AgNPs synthesized from the chitin of *M. ayliffe* scales exhibited absorption peaks approximately between the range of 3200 cm⁻¹, 2700 cm⁻¹, 1500 cm⁻¹, 1000 cm⁻¹, and 900 cm⁻¹, which is indicative of the H-bonded, H–C=O: C–H stretch, N–O asymmetric stretch, =C–H bend, and C–H band, respectively. The SEM micrographs primarily showed that the H-bonded, C=O stretch, N–O asymmetric stretch, and =C–H bend were all indicated by prominent peaks at 3400, 1700, 1600, and 1000 in the AgNPs synthesized from *P. sanguinolentus*. The findings clearly show that main amino groups were involved in the interaction with metal surfaces and that these groups served as capping sites for the stabilization of AgNPs.

Infection with *Vibrio* spp. typically happens when a person eats food that has been tainted with the bacteria from the feces of infected animals or people [39]. Egg, meat, and poultry are frequently linked to *Vibrio* spp. outbreaks, but these bacteria can also infect other foods such fruits and vegetables [40,41]. The most crucial quality of medical textiles is their antibacterial activity, which offers sufficient defense against microbes, biological fluids, aerosols, and disease transmission [42]. *Vibrio* spp., a food pathogen, was susceptible to the antibacterial activity of the chitin films. Chitin from *M. ayliffe* scales, *P. sanguinolentus*, AgNP-synthesized chitin from *M. ayliffe* scales, and AgNP-synthesized chitin from *P. sanguinolentus* were the four distinct chitin films that were tested for antibacterial activity. AgNPs produced from *M. ayliffe* scales had stronger inhibitory activity (20 mm) than other films in the current study against the food pathogen *Vibrio* spp. The electrostatic interaction between positively-charged chitin and negatively-charged bacterial cell membranes significantly alters the membranes' ability to act as barriers. They also noted that chitin's ability to act as a chelator can have an impact on microbial growth. The antibacterial action of chitin is enhanced by the use of organic acids with low carbon numbers, such as acetic acid, as a chitin solvent [43]. Therefore, it is possible that the chitin film's action will break the bacterial cell membranes, allowing for the entry of natural antioxidants into the cells. Ascorbic acid, one of the antioxidants, has antimicrobial characteristics, which can enhance the chitin film's antibacterial properties [44]. The zone of inhibition observed in this investigation indicates that cellulose film containing ascorbic acid may have inhibitory effects against *Vibrio* species.

In the application of biopolymer films and coatings for fruit and vegetable packaging, it was observed that they had positive effects on the preservation of quality and freshness of the products in terms of reducing the loss of color, vitamins, and minerals, and preserving the nutritional properties [45]. In the present study, chitin AgNPs from *M. ayliffe* scales show potential physical, mechanical, and antimicrobial properties. Of the many nanoparticles tested, chitin AgNPs of *M. ayliffe* scales show better food preservative applications. The chitin silver nanoparticles of *M. ayliffe* scales were coated as an outer layer on *Capsicum annuum* and *Solanum lycopersicum* under sterile conditions at room temperature. The result indicates that when compared to chitin nanoparticle non-coated *C. annuum* and

S. lycopersicum, chitin nanoparticle coated *C. annuum* and *S. lycopersicum* showed a good shelf life (0 to 5 days) at room temperature.

5. Conclusions

The use of natural food preservatives instead of chemical preservatives is more important for minimizing the addition of chemical additives to foods. Chitin serves as a protective covering and mechanical support to soft-bodied organisms producing it. In the present study, chitin obtained from *M. ayliffe* scales and *P. sanguinolentus* exoskeleton was characterized for its molecular and ultrastructural features. The synthesis of AgNPs using chitin AgNPs and their subsequent characterization provided crucial insights into their size, shape, and stability. Further, chitin as well as chitin-integrated AgNPs into chitin composite films exhibited substantial antimicrobial potential. The AgNP-synthesized chitin from *M. ayliffe* scales displayed remarkable inhibition activity against *Vibrio* spp. food pathogens. Moreover, the application of chitin AgNPs onto *Capsicum annuum* and *Solanum lycopersicum* successfully extended their shelf life at room temperature. This innovative approach holds significant promise for addressing the challenge of food preservation, contributing to sustainable strategies that reduce food waste and enhance food security.

Author Contributions: R.V., K.A., M.J., R.M., B.S., P.K., S.J., V.P. and L.G.; conceptualization, R.V., K.A., M.J., R.M. and B.S.; methodology, B.S., P.K., S.J. and V.P.; formal analysis, R.V., K.A., M.J., R.M., B.S., P.K., S.J., V.P. and L.G.; investigation, M.J., R.M., B.S., P.K., S.J., V.P. and L.G., R.M.S.K.; writing—review and editing, R.V., K.A., M.J., R.M., B.S., P.K., S.J., V.P., R.M.S.K. and L.G.; visualization, R.V., K.A., M.J., R.M., B.S. and P.K.; supervision: all authors. All authors have read and agreed to the published version of the manuscript.

Funding: Funded by AMET University under the AMET- Seed money project on Extraction of chitin from Marine Resources and its Biomedical Applications (No. 6670/AMET/Seed money/2019 Dt. 19.10.2019).

Data Availability Statement: The datasets used and/or analyzed during the current study are available from the corresponding author on reasonable request.

Acknowledgments: The authors express their gratitude to the management of AMET University, Chennai, for providing the research facilities to carry out this work.

Conflicts of Interest: The authors have no conflict of interest.

References

1. Massaglia, S.; Borra, D.; Peano, C.; Sottile, F.; Merlino, V.M. Consumer preference heterogeneity evaluation in fruit and vegetable purchasing decisions using the best-worst approach. *Foods* **2019**, *8*, 266. [[CrossRef](#)] [[PubMed](#)]
2. Berdegué, J.A.; Balsevich, F.; Flores, L.; Reardon, T. Central American supermarkets' private standards of quality and safety in procurement of fresh fruits and vegetables. *Food Policy* **2005**, *30*, 254–269. [[CrossRef](#)]
3. Ziv, C.; Fallik, E. Postharvest Storage Techniques and Quality Evaluation of Fruits and Vegetables for Reducing Food Loss. *Agronomy* **2021**, *11*, 1133. [[CrossRef](#)]
4. Duan, C.; Meng, X.; Meng, J.; Khan, M.I.H.; Dai, L.; Khan, A.; Ni, Y. Chitosan as a preservative for fruits and vegetables: A review on chemistry and antimicrobial properties. *J. Bioresour. Bioprod.* **2019**, *4*, 11–21. [[CrossRef](#)]
5. Rawat, S. Food Spoilage: Microorganisms and their prevention. *Asian J. Plant Sci. Res.* **2015**, *5*, 47–56.
6. Iversen, L.J.L.; Rovina, K.; Vonnie, J.M.; Matanjun, P.; Erna, K.H.; 'Aqilah, N.M.N.; Felicia, W.X.L.; Funk, A.A. The Emergence of Edible and Food-Application Coatings for Food Packaging: A Review. *Molecules* **2022**, *27*, 5604. [[CrossRef](#)] [[PubMed](#)]
7. Baranwal, J.; Barse, B.; Fais, A.; Delogu, G.L.; Kumar, A. Biopolymer: A Sustainable Material for Food and Medical Applications. *Polymers* **2022**, *14*, 983. [[CrossRef](#)]
8. Moshood, T.D.; Nawanir, G.; Mahmud, F.; Mohamad, F.; Ahmad, M.H.; AbdulGhani, A. Sustainability of biodegradable plastics: New problem or solution to solve the global plastic pollution? *Curr. Res. Green Sustain. Chem.* **2022**, *5*, 100273. [[CrossRef](#)]
9. Jianglian, D.; Shaoying, Z. Application of chitosan based coating in fruit and vegetable preservation: A review. *J. Food Process. Technol* **2013**, *4*, 227. [[CrossRef](#)]
10. Zambrano-Zaragoza, M.L.; González-Reza, R.; Mendoza-Muñoz, N.; Miranda-Linares, V.; Bernal-Couoh, T.F.; Mendoza-Elvira, S.; Quintanar-Guerrero, D. Nanosystems in edible coatings: A novel strategy for food preservation. *Int. J. Mol. Sci.* **2018**, *19*, 705. [[CrossRef](#)]

11. Seidi Damyeh, M.; Mereddy, R.; Netzel, M.E.; Sultanbawa, Y. An insight into curcumin-based photo-sensitization as a promising and green food preservation technology. *Compr. Rev. Food Sci. Food Saf.* **2020**, *19*, 1727–1759. [[CrossRef](#)] [[PubMed](#)]
12. Shiekh, R.A.; Malik, M.A.; Al-Thabaiti, S.A.; Shiekh, M.A. Chitosan as a novel edible coating for fresh fruits. *Food Sci. Technol. Res.* **2013**, *19*, 139–155. [[CrossRef](#)]
13. Dhall, R.K. Advances in edible coatings for fresh fruits and vegetables: A review. *Crit. Rev. Food Sci. Nutr.* **2013**, *53*, 435–450. [[CrossRef](#)] [[PubMed](#)]
14. Muhamad, I.I.; Zulkifli, N.; Lazim, N.A.M. Bioactive algal-derived polysaccharides: Multi-functionalization, therapeutic potential and biomedical applications. *Curr. Pharm. Des.* **2019**, *25*, 1147–1162. [[CrossRef](#)] [[PubMed](#)]
15. Bealer, E.J.; Kavetsky, K.; Dutko, S.; Lofland, S.; Hu, X. Protein and polysaccharide-based magnetic composite materials for medical applications. *Int. J. Mol. Sci.* **2020**, *21*, 186. [[CrossRef](#)] [[PubMed](#)]
16. Schmitz, C.; González Auza, L.; Koberidze, D.; Rasche, S.; Fischer, R.; Bortesi, L. Conversion of chitin to defined chitosan oligomers: Current status and future prospects. *Mar. Drugs* **2019**, *17*, 452. [[CrossRef](#)] [[PubMed](#)]
17. Balassa, L.L.; Prudden, J.F. Applications of chitin and chitosan in wound-healing acceleration. In Proceedings of the First International Conference on Chitin/Chitosan, Boston, MA, USA, 11 April 1978; National Technical Information: Springfield, VA, USA, 1978; pp. 296–305.
18. Huang, X.; Xie, W.J.; Gong, Z.Z. Characteristics and antifungal activity of a chitin binding protein from Ginkgo biloba. *FEBS Lett.* **2000**, *478*, 123–126. [[CrossRef](#)]
19. Benhabiles, M.S.; Salah, R.; Lounici, H.; Drouiche, N.; Goosen, M.F.A.; Mameri, N. Antibacterial activity of chitin, chitosan and its oligomers prepared from shrimp shell waste. *Food Hydrocoll.* **2012**, *29*, 48–56. [[CrossRef](#)]
20. Carpenter, K.E. *The Living Marine Resources of the Western Central Atlantic*; Volume 1: Introduction, molluscs, crustaceans, hagfishes, sharks, batoid fishes, and chimaeras; Food and Agricultural Organization of the United Nations: Rome, Italy, 2002.
21. Vijayaraj, R.; Altaff, K.; Lakshmanan, G.; Jayaprakashvel, M.; Mickymaray, S.; Gunapriya, R.; Alothaim, A.S. Inhibitory Activity of Chitin,(2-Acetamido-2-Deoxy-Hexopyranose) against Penicillin-Binding Proteins of Staphylococcus aureus. *Coatings* **2022**, *12*, 1854. [[CrossRef](#)]
22. Kumaran, N.; Vijayaraj, R.; Swarnakal. Biosynthesis of silver nano particles from *Leucas aspera* (willd.) link and its anti-inflammatory potential against carrageen induced paw edema in rats. *Int. J. Pharm. Sci. Res.* **2017**, *8*, 2588–2593.
23. Nadarajah, S.K.; Vijayaraj, R.; Mani, J. Therapeutic significance of *Loligo vulgaris* (Lamarck, 1798) ink extract: A biomedical approach. *Pharmacogn. Res.* **2017**, *9* (Suppl. S1), S105. [[CrossRef](#)] [[PubMed](#)]
24. Vijayaraj, R.; Sri Kumaran, N.; Altaff, K. Toxicity evaluation of novel antidiabetic compound (11-methoxy-2-methyltridecane-4-ol) from marine macro alga, *Gracilaria edulis*. *J. Biol. Act. Prod. Nat.* **2022**, *12*, 223–231. [[CrossRef](#)]
25. Valdes, A.; Ramos, M.; Beltrán, A.; Jiménez, A.; Garrigós, M.C. State of the art of antimicrobial edible coatings for food packaging applications. *Coatings* **2017**, *7*, 56. [[CrossRef](#)]
26. Kurita, K. Controlled functionalization of the polysaccharide chitin. *Prog. Polym. Sci.* **2001**, *26*, 1921–1971. [[CrossRef](#)]
27. Sharp, R.G. A review of the applications of chitin and its derivatives in agriculture to modify plant-microbial interactions and improve crop yields. *Agronomy* **2013**, *3*, 757–793. [[CrossRef](#)]
28. Zhang, M.; Haga, A.; Sekiguchi, H.; Hirano, S. Structure of insect chitin isolated from beetle larva cuticle and silkworm (*Bombyx mori*) pupa exuvia. *Int. J. Biol. Macromol.* **2000**, *27*, 99–105. [[CrossRef](#)]
29. Sajomsang, W.; Gonil, P. Preparation and characterization of α -chitin from cicada sloughs. *Mater. Sci. Eng. C* **2010**, *30*, 357–363. [[CrossRef](#)]
30. Dahmane, E.M.; Taourirte, M.; Eladlani, N.; Rhazi, M. Extraction and characterization of chitin and chitosan from *Parapenaeus longirostris* from Moroccan local sources. *Int. J. Polym. Anal. Charact.* **2014**, *19*, 342–351. [[CrossRef](#)]
31. Povea, M.B.; Monal, W.A.; Cauich-Rodríguez, J.V.; Pat, A.M.; Rivero, N.B.; Covas, C.P. Interpenetrated chitosan-poly (acrylic acid-co-acrylamide) hydrogels. Synthesis, characterization and sustained protein release studies. *Mater. Sci. Appl.* **2011**, *2*, 509. [[CrossRef](#)]
32. Qu, X.; Wirsén, A.; Albertsson, A.C. Effect of lactic/glycolic acid side chains on the thermal degradation kinetics of chitosan derivatives. *Polymer* **2000**, *41*, 4841–4847. [[CrossRef](#)]
33. Brugnerotto, J.; Lizardi, J.; Goycoolea, F.M.; Argüelles-Monal, W.; Desbrieres, J.; Rinaudo, M. An infrared investigation in relation with chitin and chitosan characterization. *Polymer* **2001**, *42*, 3569–3580. [[CrossRef](#)]
34. Kumari, S.; Rath, P.; Kumar, A.S.H.; Tiwari, T.N. Extraction and characterization of chitin and chitosan from fishery waste by chemical method. *Environ. Technol. Innov.* **2015**, *3*, 77–85. [[CrossRef](#)]
35. Gbenebor, O.P.; Adeosun, S.O.; Lawal, G.I.; Jun, S.; Olaleye, S.A. Acetylation, crystalline and morpho-logical properties of structural polysaccharide from shrimp exoskeleton. *Eng. Sci. Technol. Int. J.* **2017**, *20*, 1155–1165.
36. Amjed, N.; Bhatti, I.A.; Zia, K.M.; Iqbal, J.; Jamil, Y. Synthesis and characterization of stable and biological active chitin-based polyurethane elastomers. *Int. J. Biol. Macromol.* **2020**, *154*, 1149–1157. [[CrossRef](#)] [[PubMed](#)]
37. Jan, H.; Zaman, G.; Usman, H.; Ansir, R.; Drouet, S.; Gigliolo-Guivarc’h, N.; Abbasi, B.H. Biogenically proficient synthesis and characterization of silver nanoparticles (Ag-NPs) employing aqueous extract of *Aquilegia pubiflora* along with their in vitro antimicrobial, anti-cancer and other biological applications. *J. Mater. Res. Technol.* **2021**, *15*, 950–968. [[CrossRef](#)]
38. Ashraf, H.; Anjum, T.; Riaz, S.; Naseem, S. Microwave-assisted green synthesis and characterization of silver nanoparticles using *Melia azedarach* for the management of Fusarium wilt in tomato. *Front. Microbiol.* **2020**, *11*, 238. [[CrossRef](#)] [[PubMed](#)]

39. Yan, D.; Li, Y.; Liu, Y.; Li, N.; Zhang, X.; Yan, C. Antimicrobial Properties of Chitosan and Chitosan Derivatives in the Treatment of Enteric Infections. *Molecules* **2021**, *26*, 7136. [[CrossRef](#)]
40. Ashbolt, N.J. Microbial contamination of drinking water and disease outcomes in developing regions. *Toxicology* **2004**, *198*, 229–238. [[CrossRef](#)]
41. Azwai, S.M.; Alfallani, E.A.; Abolghait, S.K.; Garbaj, A.M.; Naas, H.T.; Moawad, A.A.; Eldaghayes, I.M. Isolation and molecular identification of *Vibrio* spp. by sequencing of 16S rDNA from seafood, meat and meat products in Libya. *Open Vet. J.* **2016**, *6*, 36–43. [[CrossRef](#)]
42. Gxalo, O.; Digban, T.O.; Igere, B.E.; Olapade, O.A.; Okoh, A.I.; Nwodo, U.U. Virulence and antibiotic re-sistance characteristics of *Vibrio* isolates from rustic environmental freshwaters. *Front. Cell. Infect. Microbiol.* **2021**, *11*, 732001. [[CrossRef](#)]
43. Mondal, A.; Dhar, A.K.; Banerjee, S.; Hasnain, M.S.; Nayak, A.K. Antimicrobial uses of chitosan. In *Chitosan in Biomedical Applications*; Academic Press: Cambridge, MA, USA, 2022; Volume 1, pp. 13–36.
44. Almasi, H.; Jafarzadeh, P.; Mehryar, L. Fabrication of novel nanohybrids by impregnation of CuO nanoparticles into bacterial cellulose and chitosan nanofibers: Characterization, antimicrobial and release properties. *Carbohydr. Polym.* **2018**, *186*, 273–281. [[CrossRef](#)]
45. Galus, S.; Kadzińska, J. Food applications of emulsion-based edible films and coatings. *Trends Food Sci. Technol.* **2015**, *45*, 273–283. [[CrossRef](#)]

Disclaimer/Publisher’s Note: The statements, opinions and data contained in all publications are solely those of the individual author(s) and contributor(s) and not of MDPI and/or the editor(s). MDPI and/or the editor(s) disclaim responsibility for any injury to people or property resulting from any ideas, methods, instructions or products referred to in the content.